Energy & Environmental Science

PAPER

View Article Online
View Journal | View Issue

CrossMark click for updates

Cite this: *Energy Environ. Sci.*, 2014, 7, 3727

Corn protein-derived nitrogen-doped carbon materials with oxygen-rich functional groups: a highly efficient electrocatalyst for all-vanadium redox flow batteries†

Minjoon Park, Jaechan Ryu, Youngsik Kim and Jaephil Cho*

Received 9th July 2014
Accepted 21st August 2014

DOI: 10.1039/c4ee02123a

www.rsc.org/ees

Recent studies on all-vanadium redox flow batteries (VRFBs) have focused on carbon-based materials for cost-effective electrocatalysts to commercialize them in grid-scale energy storage markets. We report an environmentally friendly and safe method to produce carbon-based catalysts by corn protein self-assembly. This new method allows carbon black (CB) nanoparticles to be coated with nitrogen-doped graphitic layers with oxygen-rich functionalities (N-CB). We observed increased catalytic activity of this catalyst toward both V^{2+}/V^{3+} and VO^{2+}/VO_2^{+} ions, showing a 24% increased mass transfer process and *ca.* 50 mV higher reduction onset potential compared to CB catalyst. It is believed that the abundant oxygen active sites and nitrogen defects in the N-CB catalyst are beneficial to the vanadium redox reaction by improving the electron transfer rate and giving faster vanadium ion transfer kinetics.

Broader context

All-vanadium redox flow batteries have received great attention as a possible solution for large-scale energy storage systems (ESS), first invented by M. Skyllas Kazacos in 1985. This system has several advantages such as a long life cycle, design flexibility, and safety; however, the low energy density, and poor reactivity on carbon materials are great obstacles in market penetration. We used the corn protein "zein" as a nitrogen doping source. It has been produced by the United States over a long period, as a by-product after the manufacture of corn flour, corn oil, and bio-ethanol, *etc.* This study shows that highly effective corn protein-derived nitrogen-doped carbon materials as an oxygen-rich electrocatalyst can be achieved by a safe and low-cost method. Thus, this technology with cost-effective and scalable properties is very important for its application in grid-scale energy storage systems. In addition, the application of corn protein as a heteroatom doping source will be readily adaptable for other electrode materials applied to various battery systems.

Introduction

In recent years, rechargeable grid-scale energy storage systems (ESS) such as redox flow batteries coupled with renewable energy sources have been employed to solve daily and seasonal problems, for instance, intermittency, nonlinearity and uncertainty of power input and output.[1,2] Out of the various redox flow batteries such as the lithium iodine redox battery[3] or the organic–inorganic redox flow battery,[4] the all-vanadium redox flow batteries (VRFBs) have been widely studied and successfully deployed on a commercial scale.[5] VRFBs have several advantages such as a decoupling of energy and capacity and a long life cycle. In contrast to the electrodes of conventional lithium ion batteries that store energy-bearing species in their interstitial structures, the electrodes of VRFBs only provide redox active surfaces (sites) for redox reactions without changing their structure, phase, or morphology, where vanadium redox reactions occur on the electrode surface. For this reason, a longer electrode service life can be expected in VRFBs.

In spite of several advantages, the increase in overall cell polarization at higher charge/discharge current densities during cycles in flow cells is a critical issue in attaining a high rate capability and high efficiency. The overpotentials in flow cell systems consist of ohmic polarization, charge transfer polarization, and concentration polarization resistance.[6] Bin Li *et al.* reported that the electrode material and its surface chemistry determine the system polarization characteristics such as charge transfer resistance, because the vanadium redox reaction takes place on the electrode surface.[7] They also reported that overpotentials arising from concentration polarizations remain the same, since identical electrolytes, membranes, and flow rates are used in the flow cell test. Thus, many researchers have focused on the reduction of cell overpotentials in flow cells by developing effective electrode materials and electrocatalysts.

A carbon-based material such as pristine carbon felt has been considered to be one of the most promising electrode

Department of Energy Engineering, School of Energy and Chemical Engineering, Ulsan National Institute of Science and Technology (UNIST), Ulsan, 689-798, South Korea. E-mail: jpcho@unist.ac.kr

† Electronic supplementary information (ESI) available: Table S1, and Fig. S1–S9. See DOI: 10.1039/c4ee02123a

materials for VRFBs owing to its low-cost, high stability, high conductivity, and corrosion resistance.[7,8] However, its poor kinetic reversibility and electrochemical reactivity have hampered the commercialization of VRFBs with a low current density during charge/discharge cycles.[9,10] Over the years, intensive efforts have been devoted to overcome the above-mentioned drawbacks by introducing surface functionalities for abundant active sites or increasing electron conductivities.[11] To better understand the state-of-the art of various electrocatalysts in VRFB systems, recent studies are summarized, presenting the electrochemical properties with various current densities and cycles (ESI, Table S1†).[12–17]

Metal-based catalysts (Pt,[18] Bi,[19] and Ir[17] *etc.*) deposited on carbon felt have been studied to improve the cycle performance and catalytic activity of the vanadium redox reaction. However, this approach has been discouraged because of scarcity of the metals or sensitivity to gas evolution. Recently, Pacific Northwest National Laboratory (PNNL) has reported several novel catalysts with low cost, excellent stability, and cell performance by using a bismuth nanoparticle or niobium oxide nanorod.[7,20] As an alternative strategy, modified carbon materials have been studied as effective candidates for further broad applications of VRFBs.[21] Recently, we reported on the use of carbon nanotube (CNT)/carbon nanofiber (CNF) composites as carbon-based electrocatalysts, which led to outstanding cell performance.[22] Significantly, N-doping into carbon materials, including CNTs,[14] graphene,[23] and mesoporous carbon[24] has been found to improve the vanadium redox reaction by facilitating the formation of defect sites for ion adsorption. On the other hand, difficulties with their synthesis including ammonia toxicity, high price of metal precursors, or flammability of ethylenediamine at higher temperatures hindered their mass production. This has been one of the critical issues for the commercial uptake of VRFBs. Bio-derived heteroatom-doped carbon materials have been widely studied as electrode/catalyst materials for energy devices.[25–29] Recently, to overcome these drawbacks, various amino acids such as alanine, cysteine, and glycine have been studied as a safe, non-toxic and inexpensive heteroatom doping source for electrocatalysts.[30]

We have proposed a new synthesis process for highly active carbon-based electrocatalysts using the corn protein "zein". Zein is a major protein in corn and has been produced in the United States in great quantities and at a low cost ($10 per kg).[31,32] The composition of zein protein can be classified as 50% hydrophobic amino acids including alanine, proline and leucine, providing nitrogen for growing kernels (Fig. S1†). This material mainly contains a high α-helix content with β-sheet fractions.[33] In addition, the zein molecule has a unique structure with amphiphilic characteristics,[34,35] which is one of the main driving forces to form ordered-film structures without external action and their self-organization into two-dimensional periodic structures.[36]

In this work, inspired by previous research on zein self-assembly, bio-derived nitrogen-doped carbon black particles, denoted as N-CB catalyst, were fabricated, which have abundant active oxygen sites and nitrogen defects for vanadium redox reactions. Without supplying any external nitrogen containing gases or metal seeds, the rearrangement of zein molecules and the film forming behavior facilitated the formation of hetero-atom doping on the surface of the CB particles. To the best of our knowledge, this is the first attempt to use corn protein as a doping source and to prepare nitrogen-doped carbon materials by zein self-assembly.

Experimental

Catalyst design and synthesis

The N-CB catalyst was made by the simple solution method involving the evaporation-induced self-assembly process (EISA) in binary solvent. First, 0.1 g of zein powder (Zein, Sigma-Aldrich) was stirred into a mixed solvent composed of 7 mL of ethanol and 3 mL of DI water, and a yellow colored zein solution was obtained after 10 minutes of stirring. The zein solution was blended with 0.3 g of carbon black (Ketjen black, EC-600JD, AkzoNobel) particles, resulting in the formation of a zein coating on the carbon black particles. In addition, various compositions of zein and carbon black powder (1 : 1, 1 : 3, 2 : 3, 1 : 8, and 1 : 15) were prepared at 800 °C in Ar to determine the optimum ratio. The selected composition was 1 : 3, the optimum ratio according to the electrochemical results as shown in Fig. S7.† This binary solvent was evaporated at 60 °C to allow the zein to self-assemble on the CB surface by forming zein thin films. Next, the remaining powders were placed in a tube furnace and fired for 3 h at various temperatures (700, 800, and 900 °C) in an Ar atmosphere. Finally, the N-CB catalyst composites were obtained after the furnace had cooled down to room temperature. For comparison, pristine carbon black was also heat-treated at the above-mentioned temperatures as a control sample.

Electrochemical measurements

Cyclic voltammetry measurements were made using a typical three-electrode cell. Carbon felt as working electrode with a diameter of 6 mm was connected to a platinum wire with a reference electrode (Ag/AgCl), and counter electrode (Pt wire) in 0.1 M $VOSO_4$ (Sigma-Aldrich, 99.5%) in 3 M H_2SO_4 solution (Sigma-Aldrich, 98%) at different scan rates ranging from 1 to 10 mV s^{-1}. A single cell was assembled for charge/discharge tests (ESI, Fig. S8†). The positive electrolyte was prepared by dissolving 2 M $VOSO_4$ in 3 M H_2SO_4 solution. The negative electrolyte was also prepared by electrolysis of 2 M $VOSO_4$ in 3 M H_2SO_4 solution, then 20 mL of positive and negative electrolyte was used in a charge/discharge test, respectively. The untreated and prepared electrodes (active area of 5 cm^2) with a thickness of 3 mm were used as the positive and negative electrode, respectively, and compressed into a thickness of 2 mm when stacking electrodes. Nafion117 ion exchange membrane was employed and a graphite-based plate was placed between the electrode and copper current collectors. The test cell was charged and discharged under the operating potential range of 1.65 to 0.8 V with a current density range of 50 to 150 mA cm^{-2} and with a flow rate of 50 mL min^{-1}.

Characterization

Scanning electron microscopy (SEM) and transmission electron microscopy (TEM) images were collected using a FE-SEM (S-4800, Hitachi) operating at 10 kV and HR-TEM (JEM2100, JEOL) operating at 200 kV, respectively. Elemental mapping was performed using energy-dispersive X-ray spectroscopy coupled to the TEM. XRD patterns were obtained on an X-ray diffractometer (D/Max2000, Rigaku). Surface chemistry was examined by X-ray photoelectron spectroscopy (Thermo Fisher, UK). Raman spectra were collected on a Micro-Raman (WITec) with 532 nm laser. BET measurement was used to determine the specific surface area of the electrodes (ASAP2420, Micromeritics). A potentiostat/galvanostat (WBC3000, WonAtech) was used to evaluate the electrochemical properties. The electrochemical impedance spectrum (EIS) was measured on a single potentiostat (Ivium) by applying an alternating voltage of 5 mV over the frequency ranging from 10^{-2} to 10^{5} Hz.

Electrode fabrication

The N-CB carbon felt electrode was made by coating the prepared catalyst on the carbon felt (PAN CF-20-3, Nippon carbon) surface and drying at 60 °C. First, the N-CB catalyst ink was prepared by dissolving 20 mg of N-CB particles in a mixture of 100 μL of 5 wt% Nafion (Sigma-Aldrich), and 900 μL of ethanol, then followed by ultrasonically blending for 20 min. The CB catalyst ink was fabricated by an identical process. Then 5 mg cm^{-2} of catalyst ink was coated onto a carbon felt to produce the distributed catalyst layer, and then dried at 60 °C for 12 h. The 5 cm^2 electrodes were placed in a single cell on both the negative and positive sides for charge/discharge cycling tests.

Results and discussion

The effective active site for the redox reaction of vanadium ions and excellent electron conductivity of the electrode are the key parameters in the increased mass transfer rate and electron transfer kinetics toward vanadium redox couples.[23] To promote the electrochemical properties of the electrode, we coated the carbon black with zein protein by the evaporation-induced self-assembly method (EISA).[36] After carbonization of the zein in an inert atmosphere (Fig. 1a), it can provide more effective oxygen-rich active sites for the vanadium redox reaction, and develop electron conductive networks by forming a nitrogen-doped layer. This functionalized coating layer can contribute to the enhancement in cell performance by improving the vanadium redox reaction during charge and discharge at high current rates.

The synthesis process for the oxygen-rich, nitrogen-doped coating layer on CB using the zein self-assembly is environmentally friendly, simple and highly scalable. Briefly, the N-CB catalyst was prepared by a simple solution method involving the EISA method in binary solvents, followed by a heat treatment (Fig. 1b) (see Experimental section for a detailed description).

The mechanism of formation of a self-assembled zein film on carbon black particles is presented in Fig. 2a. The molecular structure of zein has been studied previously. When dissolved in ethanol/water it consisted of *ca.* 80% α-helix clusters in the initial stage.[36] The content of α-helix in solvents could be controlled by varying the concentration of solutes and the volume ratio of solvents. The β-sheet structure formed from the α-helix cluster could be arranged by controlling the evaporation rate of the binary solvents during the EISA process. This led to the change in solvent polarity by the hydrophilic conditions, which drove the self-assembly of zein molecules. Wang and Padua reported that nano-sized zein sphere, hexagonal, and lamellar phases were formed by packing an energetically favorable β-sheet structure. This was presented in TEM images where antiparallel β-sheets were packed side-by-side to form long ribbons with a periodic distance of 0.35 nm.[36] Finally, the carbon black nanoparticles could be coated by the zein ribbons interacting with the β-sheets, followed by the carbonization treatment to obtain the N-doped CB particles.

Fig. 2b presents SEM images of the pristine zein powder (upper panel) and untreated CB particles (lower panel). Typically, the CB nanoparticles have a mesoporous structure with an average diameter of ~50 nm, which can facilitate the vanadium ion adsorption by providing large active sites. As presented in Fig. 2c, the N-CB catalyst was successfully coated on the carbon felt surface (inset image: untreated carbon felt surface with a diameter ~7 μm). The N-CB catalyst was well distributed on the carbon felt as observed in the magnified SEM image (dashed circle in Fig. 2c). The HR-TEM image of the N-CB catalyst shows each CB nanoparticle is aggregated by the functionalized graphitic layers (Fig. 2d). The magnified image of Fig. 2d presents the defective graphitic surface with 0.34 nm spacing between adjacent lattice planes (Fig. S2b†). As a result, the surface morphology of the N-CB catalyst was not significantly changed when treated with zein protein (Fig. S2†). The specific surface area of the N-CB catalyst was also measured at *ca.* 984.5 $m^2 g^{-1}$ (Fig. S3†). It is thought that N-CB catalyst can sufficiently contribute to the better electrochemical performance with large surface areas. The change in the surface chemistry was examined by EDXS, XPS and Raman analysis. Energy dispersed X-ray spectroscopy (EDXS) showed that the oxygen and nitrogen atoms were successfully incorporated into the N-CB particles, which could act as highly reactive active sites for vanadium redox couples (Fig. S4†). Raman spectroscopy was also conducted to further study the microstructure of the obtained samples (Fig. 3). The peaks at 1340 cm^{-1} and 1590 cm^{-1} correspond to the D and G bands of typical carbon materials.[37] In the first-order region of the two strong bands, the intensity of the defect-induced D band is much higher than that of the G band, indicating that there were relatively abundant exposed-graphitic defects that could serve as redox active sites in both carbon black and N-CB samples. However, a higher D/G intensity ratio was observed in the N-CB catalyst due to the oxygen-rich functional groups and more defective N-doped layers. This implies that the oxygen and nitrogen functionalities could facilitate the formation of reactive defect sites for vanadium redox ions.[38]

X-ray photoelectron spectroscopy (XPS) analysis (Fig. 4) indicated the presence and chemical structures of oxygen and

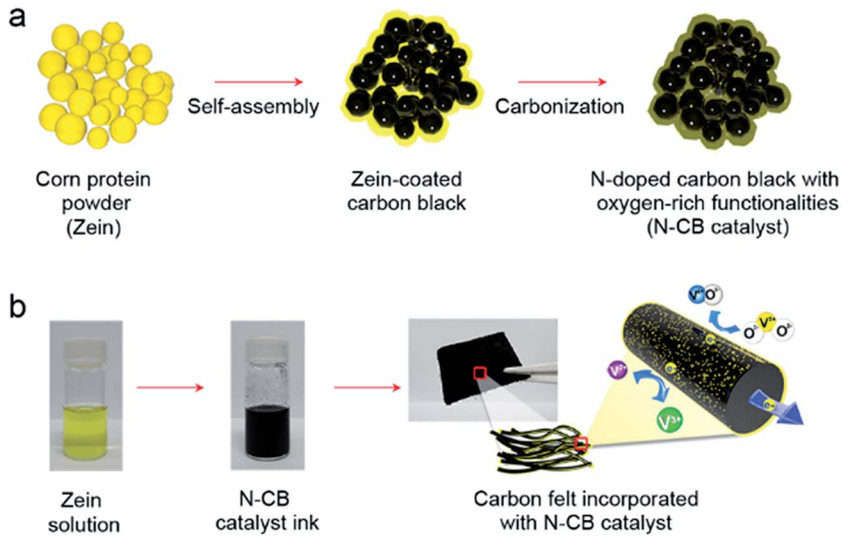

Fig. 1 (a) Schematic diagram of the N-CB catalyst fabrication process. (b) Zein powder was dissolved in a binary solvent, then CB was immersed in the solution. As the solution was evaporated in an oven, zein self-assembled on the CB. The dried powders were converted into the N-CB catalyst by carbonization at 800 °C in an argon atmosphere, then the catalyst ink was prepared by blending the N-CB in Nafion suspension in ethanol. Finally, the carbon felt was coated with the N-CB catalyst using the prepared ink.

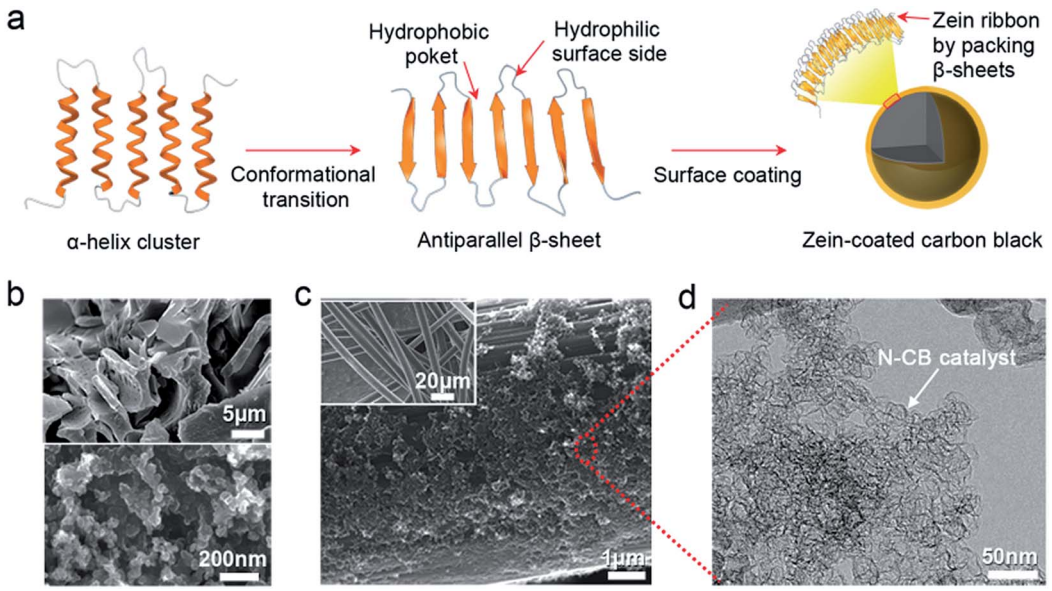

Fig. 2 (a) Possible mechanism for self-assembly of the zein coated CB nanoparticles. (b) SEM image of the pristine zein powder (upper) and the pristine CB nanoparticles (lower). (c) SEM image of the carbon felt surface coated with the N-CB catalyst. Inset image of the untreated carbon felt. (d) HR-TEM image of the N-CB catalyst.

nitrogen atoms on the surface of the catalyst samples, where all spectra were calibrated by the C1s peak of carbon at 284.2 eV. The chemical composition ratio of each functional group is also presented in Fig. S5.† Compared with untreated CB, the XPS survey of N-CB presents a predominant C1s signal with a much stronger O1s peak at 531 eV, arising from oxygen-containing species in the zein molecules. The high-resolution C1s spectrum of pristine zein shows a relatively weak energy intensity of the double-bonded carbon peak, whereas the corresponding high-resolution C1s spectra observed in the untreated CB and N-CB catalyst exhibit a sharp graphitic carbon peak at 284.2 eV (Fig. 4b). As shown in Fig. 4c, the O1s peaks in the N-CB catalyst assigned to 532.9, 531.8, and 530.6 eV can be attributed to C–C=O, C–OH, and C=O, respectively,[39] indicating increased incorporation of oxygen functional groups on the carbon black surface. They can act as the main active sites for vanadium redox couples. More specifically, the content of C–C=O functional groups in the N-CB sample, which is directly associated with vanadium redox sites, was increased by more than 27% when compared to that of the CB sample. As shown in

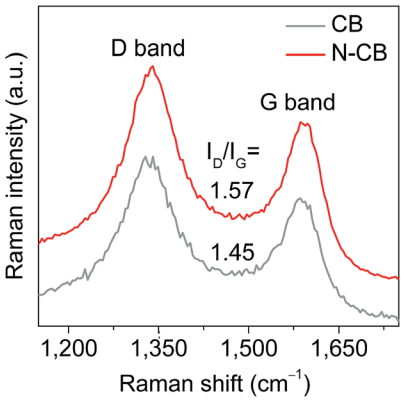

Fig. 3 Raman spectroscopy of the CB and N-CB catalyst.

Fig. 4d, no significant signals were found in the N1s region in the untreated CB sample, whereas the nitrogen-containing groups in the N-CB sample were observed with a noticeable increase in N1s signal at 400 eV. The nitrogen content in the N-CB catalyst was 1.62 at.% according to XPS analysis. The N1s region can be deconvoluted into four peaks assignable to the oxygenated-N (402.9 eV), graphitic-N (401.1 eV), pyrrolic-N (400.0 eV), and pyridinic-N (398.3 eV), respectively (Fig. 4d).[40] These nitrogen species in the carbon materials have been known to produce the defects in the graphite layer, contributing to the improvement in catalytic activity toward vanadium ions.[23] Thus, the N-doping defects in the N-CB catalyst can serve an important role in vanadium redox reactions by forming the vanadium ion adsorption sites.

Cyclic voltammetry tests were performed on the three-electrode cell system to characterize the electrochemical properties of the N-CB catalyst. The test cell was composed of negative and positive vanadium electrolytes in which carbon felt (CF) electrode, platinum wire, and Ag/AgCl were used as working, counter, and reference electrodes, respectively (detailed in the Experimental section). There are several parameters that can estimate catalytic activities for vanadium redox reactions, for instance, the potential difference (ΔV), the ratio of oxidation and reduction peak current (I_{pa}/I_{pc}), and the redox onset potential. As shown in Fig. 5a, the redox potential difference of the oxidized carbon felt (OCF) electrode (ΔV = 353 mV) is substantially larger than that for carbon felt coated with carbon black (CB–CF) (ΔV = 195 mV), implying that it has poor electrochemical reversibility. As for the ratio of the redox peak current (I_{pa}/I_{pc}), the OCF electrode (I_{pa}/I_{pc} = 1.54) presents an unstable vanadium redox reaction compared to the CB–CF electrode (I_{pa}/I_{pc} = 1.10). The onset redox potential for CB–CF was much higher than that of the OCF electrode. We used the N-CB catalyst that was heat-treated at 800 °C as the optimized working electrode because it exhibited the best anodic and cathodic peak current density (I_{pa} = 86.3 and I_{pc} = −75.1 mA cm^{-2}) and the lowest onset potential (see Fig. S7b†). As shown in Fig. 5a, the pronounced redox peaks corresponding to the oxidation and reduction of VO^{2+} and VO_2^+ ions are presented in the cyclic voltammograms. These peaks appeared in the carbon felt coated with the CB or N-CB samples, whereas a weak reduction peak at 0.75 V (*vs.* Ag/AgCl) was observed in the untreated carbon felt. Significantly, the reduction onset potential measured from the N-CB carbon felt electrode was around 50 mV higher than that for the CB carbon felt sample (Fig. 5a, inset). This suggests that the improved catalytic activity is originating from the N-CB catalyst. Furthermore, the peak potential difference associated with the polarization of the N-CB carbon felt electrode decreased to 146 mV at a scan rate of 5 mV s^{-1}. This implies the enhanced reversibility for vanadium

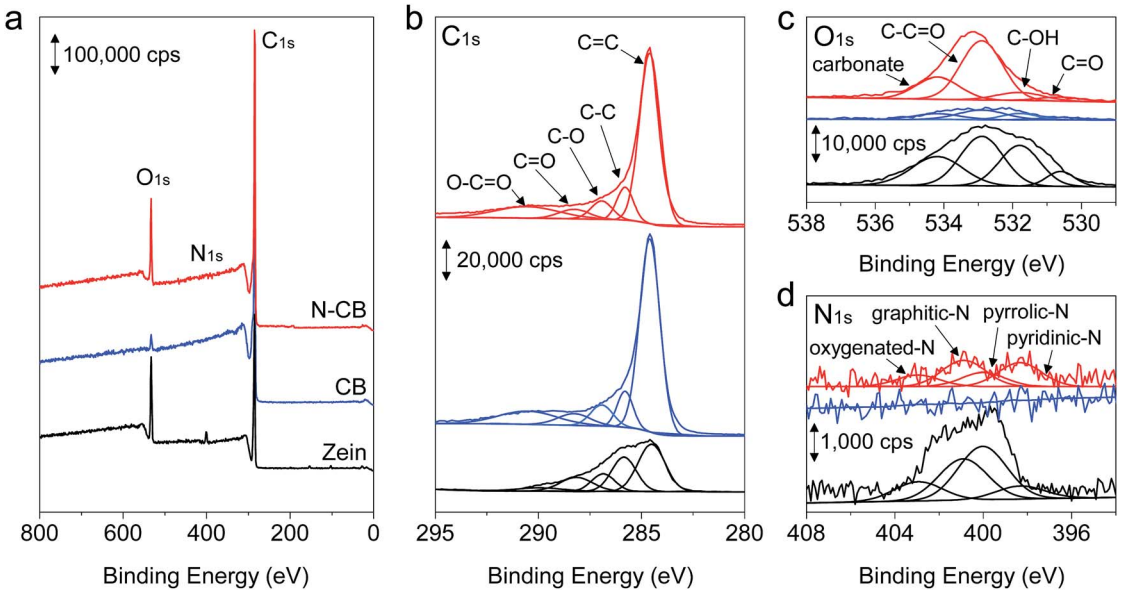

Fig. 4 (a) XPS survey of the pristine zein, CB, and N-CB catalyst. XPS analysis and its fitting from high resolution (b) C1s peak, (c) O1s peak, and (d) N1s peak.

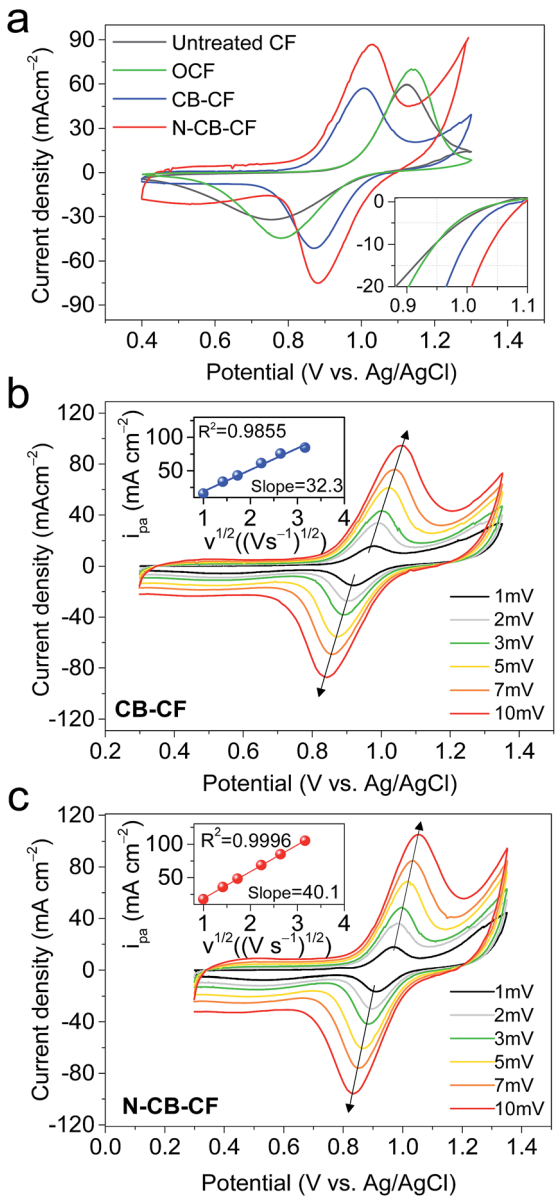

Fig. 5 (a) Cyclic voltammograms (CVs) of the untreated, oxidized, CB, and N-CB carbon felt at a scan rate of 5 mV s^{-1} with potential window of 0.4 to 1.3 V *versus* Ag/AgCl. CVs of the (b) CB carbon felt and (c) N-CB carbon felt at different scan rates. Insets: plot of the anodic peak current (I_{pa}) *versus* the square root of each scan rate. CF: carbon felt.

redox reactions. As for the negative redox reaction involving V^{2+}/V^{3+} ions, distinct anodic and cathodic peaks of the N-CB carbon felt were observed at −0.21 V and −0.71 V (*vs.* Ag/AgCl), respectively, while there were no pronounced anodic and cathodic peaks for the untreated carbon felt electrode (Fig. S6†). When the cyclic voltammogram of each sample was compared, the onset potential and potential difference of the N-CB carbon felt were much lower than those of the CB carbon felt at both negative and positive vanadium redox reactions. This improved electrochemical behavior could be caused by improved electron transfer and sufficient vanadium redox active sites owing to oxygen-rich and nitrogen-doped graphitic layers. Electrochemical impedance spectroscopy (EIS) analysis also agreed with the results of the cyclic voltammetry tests, suggesting that the formation of the electrically conductive network introduced by the functionalized graphitic layer could reduce the electron transfer resistance by *ca.* 26% (Fig. S6d†).

The mass transfer properties can be assessed by plotting the peak current density *versus* the square root of scan rate from the Randles–Sevcik equation.[41] Fig. 5b and c show the cyclic voltammetry tests, which were conducted with scan rates increasing from 1 mV s^{-1} to 10 mV s^{-1} in 0.1 M $VOSO_4$ + 3 M H_2SO_4 solutions. The value of the coefficient of determination (R^2) in the inset in Fig. 5c was close to 99%, implying that a diffusion process controls the vanadium redox reaction on the N-CB carbon felt electrode. In addition, the slope of the N-CB carbon felt electrode (Fig. 5c) is 24% larger than that of the CB carbon felt electrode (Fig. 5b), suggesting that a faster mass transfer process could be achieved on the N-CB carbon felt electrode. The improved mass transfer reaction on the N-CB catalyst could be ascribed to its high electrochemical surface area and lower surface energy induced by the heteroatom doped coating layer.

To demonstrate the practical application of the prepared catalyst, we used the carbon felt electrode incorporated with the N-CB catalyst as the negative and positive electrodes in an all-vanadium redox flow battery. We assembled flow-type single cells to evaluate the electrochemical performances of the untreated, CB, and N-CB carbon felt electrodes. The cell body was assembled using Nafion 117 (the proton exchange membrane), copper plates (the current collectors) and graphite-based bipolar plate that protect the current collectors from acidic electrolytes (detailed in Fig. S8† and Experimental section). Electrolytes consisting of 20 mL of 2 M V^{3+} and 20 mL of V^{4+} based on 3 M H_2SO_4 solutions were used as the negative and positive electrolytes, respectively.

Fig. 6a and b show the voltage profiles of the CB carbon felt and N-CB carbon felt electrodes, respectively, between 0.8 and 1.65 V at various charge–discharge current densities. The N-CB carbon felt electrode presented improved discharge capacities of 19.2 and 10.1 A h L^{-1} at current densities of 50 and 150 mA cm^{-2}, respectively (see Fig. 7b). Additionally, the N-CB catalyst exhibited a stable cycling performance for 100 cycles at 50 mA cm^{-2} as depicted in Fig. 6c. This catalyst also presented an energy efficiency (coulombic efficiency × voltage efficiency) of 85.2% at the end of 100 cycles corresponding to 450 h (4.5 h per cycle). The coulombic efficiency is the difference between the charge and discharge capacity. Likewise, the voltage efficiency is the ratio of charge and discharge voltage. After the initial charge–discharge rate of 50 mA cm^{-2} for 5 cycles, we gradually increased the current density to 150 mA cm^{-2}. The N-CB carbon felt electrode showed an energy efficiency of 86.7% at 50 mA cm^{-2} and 68.6% at a rate of 150 mA cm^{-2}. The origin of the enhanced rate capability for the N-CB catalyst during battery cycling can possibly be attributed to the significantly reduced polarization by increased redox active sites towards vanadium ions for the fast electron and mass transfer reactions. Next, to evaluate the stability of the N-CB catalyst, we swiftly changed the charge–discharge rate from 150 to 50 mA cm^{-2} (Fig. 6c).

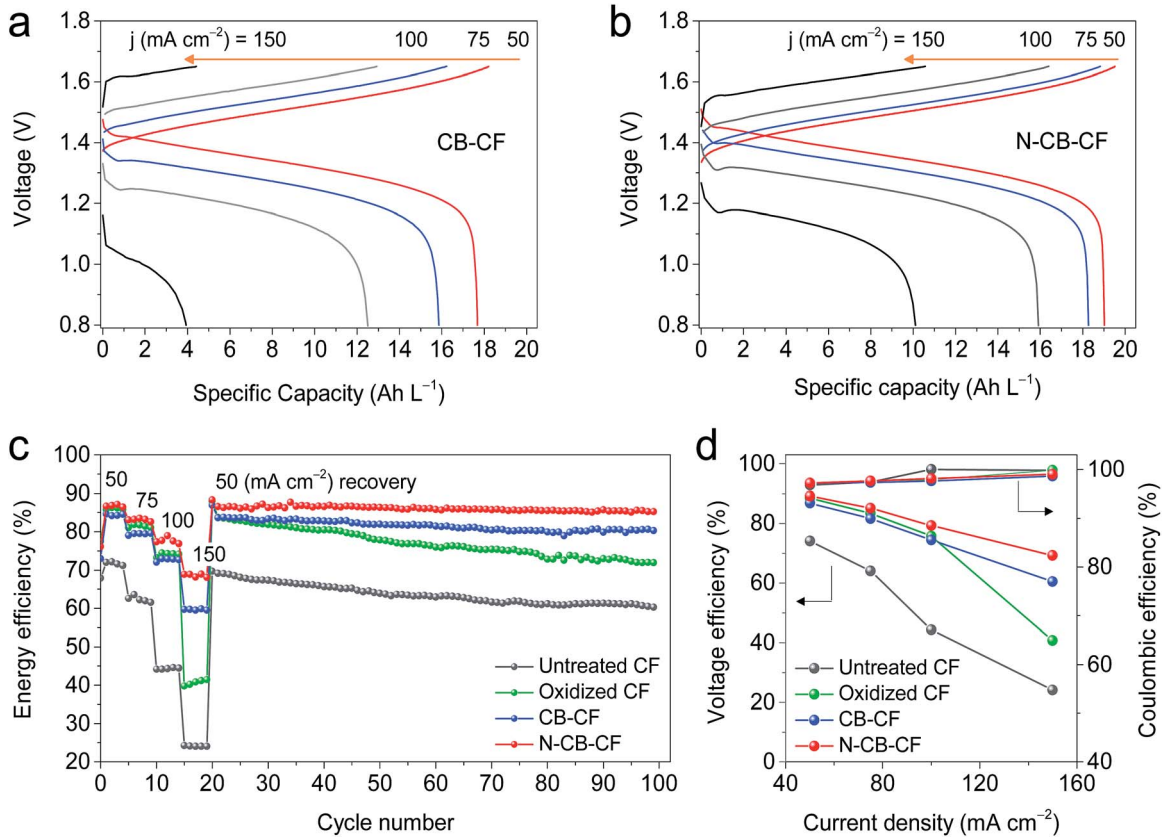

Fig. 6 Electrochemical cycling performance of (a) CB-CF and (b) N-CB-CF electrodes, and (c) Energy efficiency and (d) Voltage efficiency of the untreated CF, oxidized CF, CB-CF, and N-CB-CF electrodes during the rate capability test. CF: carbon felt.

Notably, the initial energy efficiency was remarkably recovered. This indicates the electrochemical and chemical robustness of the N-CB catalyst in concentrated acidic vanadium electrolytes. As shown in Fig. S9,† we also confirmed the stable adhesion of N-CB catalyst on carbon felt electrode after 100 cycles. The coulombic efficiency and voltage efficiency values were highest in N-CB samples, as shown in Fig. 6d.

We demonstrated that the N-CB catalyst incorporated carbon felt electrode dramatically improved the electrochemical performance of the VRFB system. These exceptional electrochemical properties can be attributed to the surface functionalized carbon black synthesized by corn protein self-assembly. The conductive and continuous graphitic coating layer of the N-CB catalyst, as well as its high surface area with surface oxygen and nitrogen functional groups help to improve the electrocatalytic activities for the vanadium redox reaction. To elucidate the surface redox reaction mechanism, the oxidized carbon felt thermally activated at 500 °C for 5 h in air atmosphere was used as the control electrode in an identical flow battery cell. The experimental results for the oxidized carbon felt were obtained and compared to those of the N-CB carbon felt electrode as shown in Fig. 7. Fig. 7a shows that the atomic content ratio of oxygen to carbon atoms in the oxidized CF electrode is *ca.* 0.22, that is two times higher than that of the N-CB carbon felt sample (*ca.* 0.10). This control electrode with high oxygen content can be expected to provide much more vanadium active sites. The improved redox current peak of the oxidized carbon felt electrode compared with that of the low oxygen containing CB carbon felt was confirmed in the cyclic voltammogram (Fig. 5a). Furthermore, the cycle performance test of the oxidized carbon felt (Fig. 7b) shows increased discharge capacity at an initial stage owing to the presence of abundant oxygen functional groups. However, there is no apparent capacity improvement at higher charge–discharge current rate for the oxidized carbon felt sample because of the lowered electron conductivity. This may be caused by the excess surface functional groups of the oxidized carbon felt, which leads to the increase in cell overpotential. In contrast, the carbon felt coated with carbon black, known as a conductive carbon composed of a large amount of sp^2 hybridized carbon (C=C), successfully presented the capacity retention even at higher current densities, but it showed a low capacity retention. This low capacity is mainly caused by the insufficient number of surface active sites for the vanadium redox reaction on the CB–CF electrode with the low the O/C ratio of *ca.* 0.02 (Fig. 7b). This result is also consistent with the cyclic voltammetry test. It is worth mentioning that the balance between the surface vanadium active sites (toward V^{2+}/V^{3+} and VO^{2+}/VO_2^{+} ions) and the electron conductivity may be of importance for developing high performance electrocatalysts in VRFB systems. Thus, the N-CB catalyst could be one of the ideal electrocatalysts in a high-performance flow battery system owing to its high surface area with an

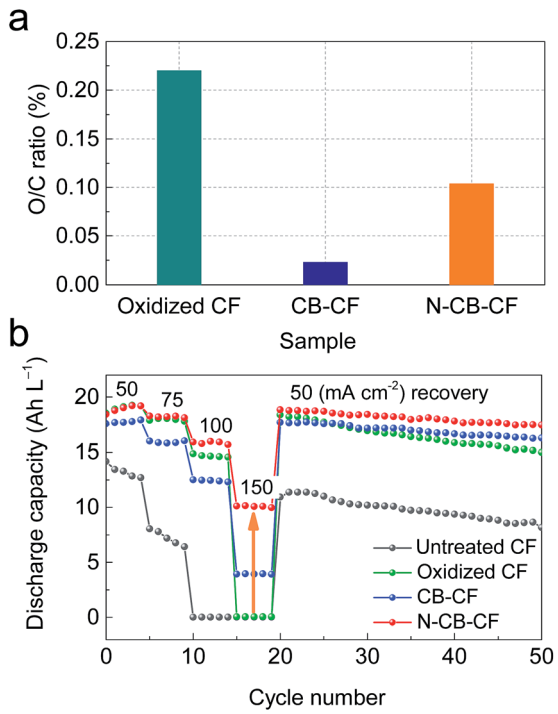

Fig. 7 (a) Chemical composition ratio of oxygen and carbon atoms for oxidized, CB, and N-CB carbon felt electrodes. (b) Discharge cycling performance.

oxygen-rich (content of *ca.* 10 wt%) and N-doped coating layer. It exhibited a significant improvement in battery performance as evident from the cyclic voltammograms and battery cycling tests.

In addition, N-doping into carbon materials has been found to promote vanadium redox reactions by the high negatively charged electron density of the incorporated nitrogen atom.[23] Accordingly, the doped nitrogen atoms as defect sites originating from the zein protein could create a lone pair of electron localized states on the carbon black surface. This eventually facilitates the electron transfer and vanadium ion adsorption steps, resulting in a high rate capability at 150 mA cm^{-2} and stable capacity retention. In addition, the origin of catalytic activity among the four different nitrogen species was examined by high-resolution N1s spectra (Fig. 8) and cyclic voltammograms (Fig. S7b†). Compared with the relationship between the content of each nitrogen species and the electrochemical catalytic activity, it was proportional to the content of graphitic (quaternary) nitrogen, centered at 401.1 eV. Such results are consistent with previous studies reporting that the graphitic nitrogen is highly stable under acidic conditions and less susceptible to protonization.[23] Therefore, we can reasonably conclude that the stable nitrogen defects on the N-CB catalyst play an important role in efficiently promoting the adsorption of vanadium redox couples.

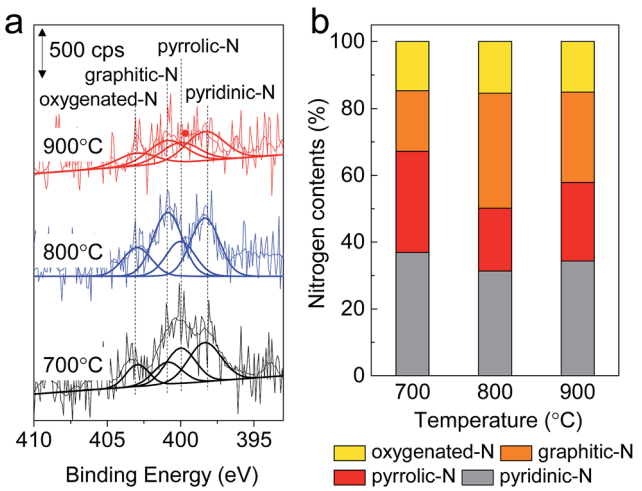

Fig. 8 (a) *Ex situ* XPS analysis of N-CB catalyst prepared at various temperatures (700, 800, and 900 °C) and (b) chemical composition ratio of N-CB catalyst from N1s spectra.

Conclusion

In summary, we have developed a highly efficient carbon-based electrocatalyst for high-performance VRFBs by an inexpensive, environmentally friendly, and safe synthesis method. The amphiphilic properties of the zein protein enabled it to self-assemble on the CB nanoparticles by the EISA process, which led to an N-doped coating layer on the CB nanoparticles. As a result, the N-CB has a high surface area with abundant oxygen functional groups, N-doped coating networks for vanadium active sites, and high electron conductivity. Compared with the CB catalyst, the N-CB catalyst exhibits excellent catalytic activity towards vanadium redox reactions owing to its oxygen-rich high surface area, nitrogen functionality for an enhanced rate of electron transfer, and faster vanadium ion transfer kinetics.

Acknowledgements

This research was supported by MSIP (Ministry of Science, ICT & Future Planning), Korea, under the C-ITRC (Convergence Information Technology Research Center) support program (NIPA-2013-H0301-13-1009) supervised by the NIPA (National IT Industry Promotion Agency).

References

1 Z. Yang, J. Zhang, M. C. Kintner-Meyer, X. Lu, D. Choi, J. P. Lemmon and J. Liu, *Chem. Rev.*, 2011, **111**, 3577–3613.
2 J. Liu, J.-G. Zhang, Z. Yang, J. P. Lemmon, C. Imhoff, G. L. Graff, L. Li, J. Hu, C. Wang, J. Xiao, G. Xia, V. V. Viswanathan, S. Baskaran, V. Sprenkle, X. Li, Y. Shao and B. Schwenzer, *Adv. Funct. Mater.*, 2013, **23**, 929–946.
3 Y. Zhao, M. Hong, N. Bonnet Mercier, G. Yu, H. C. Choi and H. R. Byon, *Nano Lett.*, 2014, **14**, 1085–1092.
4 B. Huskinson, M. P. Marshak, C. Suh, S. Er, M. R. Gerhardt, C. J. Galvin, X. Chen, A. Aspuru-Guzik, R. G. Gordon and M. J. Aziz, *Nature*, 2014, **505**, 195–198.
5 B. Dunn, H. Kamath and J. M. Tarascon, *Science*, 2011, **334**, 928–935.

6 Q. Liu, A. Turhan, T. A. Zawodzinski and M. M. Mench, *Chem. Commun.*, 2013, **49**, 6292–6294.
7 B. Li, M. Gu, Z. Nie, Y. Shao, Q. Luo, X. Wei, X. Li, J. Xiao, C. Wang, V. Sprenkle and W. Wang, *Nano Lett.*, 2013, **13**, 1330–1335.
8 K. J. Kim, Y.-J. Kim, J.-H. Kim and M.-S. Park, *Mater. Chem. Phys.*, 2011, **131**, 547–553.
9 C. Ding, H. Zhang, X. Li, T. Liu and F. Xing, *J. Phys. Chem. Lett.*, 2013, **4**, 1281–1294.
10 B. Sun and M. Skyllas-Kazacos, *Electrochim. Acta*, 1992, **37**, 2459–2465.
11 W. Wang, Q. Luo, B. Li, X. Wei, L. Li and Z. Yang, *Adv. Funct. Mater.*, 2013, **23**, 970–986.
12 G. J. Wei, C. K. Jia, J. G. Liu and C. W. Yan, *J. Power Sources*, 2012, **220**, 185–192.
13 L. Yue, W. S. Li, F. Q. Sun, L. Z. Zhao and L. D. Xing, *Carbon*, 2010, **48**, 3079–3090.
14 S. Wang, X. Zhao, T. Cochell and A. Manthiram, *J. Phys. Chem. Lett.*, 2012, **3**, 2164–2167.
15 C. A. Yao, H. M. Zhang, T. Liu, X. F. Li and Z. H. Liu, *J. Power Sources*, 2012, **218**, 455–461.
16 K. J. Kim, M. S. Park, J. H. Kim, U. Hwang, N. J. Lee, G. Jeong and Y. J. Kim, *Chem. Commun.*, 2012, **48**, 5455–5457.
17 W. H. Wang and X. D. Wang, *Electrochim. Acta*, 2007, **52**, 6755–6762.
18 T. M. Tseng, R. H. Huang, C. Y. Huang, K. L. Hsueh and F. S. Shieu, *J. Electrochem. Soc.*, 2013, **160**, A690–A696.
19 Z. González, A. Sánchez, C. Blanco, M. Granda, R. Menéndez and R. Santamaría, *Electrochem. Commun.*, 2011, **13**, 1379–1382.
20 B. Li, M. Gu, Z. Nie, X. Wei, C. Wang, V. Sprenkle and W. Wang, *Nano Lett.*, 2014, **14**, 158–165.
21 P. X. Han, Y. H. Yue, Z. H. Liu, W. Xu, L. X. Zhang, H. X. Xu, S. M. Dong and G. L. Cui, *Energy Environ. Sci.*, 2011, **4**, 4710–4717.
22 M. Park, Y. J. Jung, J. Kim, H. I. Lee and J. Cho, *Nano Lett.*, 2013, **13**, 4833–4839.
23 J. Jin, X. Fu, Q. Liu, Y. Liu, Z. Wei, K. Niu and J. Zhang, *ACS Nano*, 2013, **7**, 4764–4773.
24 Y. Shao, X. Wang, M. Engelhard, C. Wang, S. Dai, J. Liu, Z. Yang and Y. Lin, *J. Power Sources*, 2010, **195**, 4375–4379.
25 D. Oh, J. Qi, Y. C. Lu, Y. Zhang, Y. Shao-Horn and A. M. Belcher, *Nat. Commun.*, 2013, **4**, 2756.
26 Y. Zhao, F. Sakai, L. Su, Y. Liu, K. Wei, G. Chen and M. Jiang, *Adv. Mater.*, 2013, **25**, 5215–5256.
27 Z. G. Wang and B. Ding, *Adv. Mater.*, 2013, **25**, 3905–3914.
28 X. Y. Chen, C. Chen, Z. J. Zhang and D. H. Xie, *J. Mater. Chem. A*, 2013, **1**, 10903.
29 H. Zhu, J. Yin, X. Wang, H. Wang and X. Yang, *Adv. Funct. Mater.*, 2013, **23**, 1305–1312.
30 C. H. Choi, S. H. Park and S. I. Woo, *Green Chem.*, 2011, **13**, 406.
31 J. Luecha, A. Hsiao, S. Brodsky, G. L. Liu and J. L. Kokini, *Lab Chip*, 2011, **11**, 3419–3425.
32 J. W. Lawton, *Cereal Chem.*, 2002, **79**, 1–18.
33 Y. Wang and G. W. Padua, *Langmuir*, 2010, **26**, 12897–12901.
34 N. Matsushima, G.-i. Danno, H. Takezawa and Y. Izumi, *Biochim. Biophys. Acta, Gen. Subj.*, 1997, **1339**, 14–22.
35 P. Argos, K. Pedersen, M. D. Marks and B. A. Larkins, *J. Biol. Chem.*, 1982, **257**, 9984–9990.
36 Y. Wang and G. W. Padua, *Langmuir*, 2012, **28**, 2429–2435.
37 A. C. Ferrari and D. M. Basko, *Nat. Nanotechnol.*, 2013, **8**, 235–246.
38 Y. Li, W. Zhou, H. Wang, L. Xie, Y. Liang, F. Wei, J. C. Idrobo, S. J. Pennycook and H. Dai, *Nat. Nanotechnol.*, 2012, **7**, 394–400.
39 W. Li, J. Liu and C. Yan, *Electrochim. Acta*, 2011, **56**, 5290–5294.
40 K. Gong, F. Du, Z. Xia, M. Durstock and L. Dai, *Science*, 2009, **323**, 760–764.
41 R. H. Huang, C. H. Sun, T. m. Tseng, W. k. Chao, K. L. Hsueh and F. S. Shieu, *J. Electrochem. Soc.*, 2012, **159**, A1579–A1586.